Earthquake-triggered rock slope failures: Damage and site effects

J.R. Moore, V. Gischig, F. Amann, & M. Hunziker
Department of Earth Sciences, ETH Zurich, Switzerland

J. Burjanek
Swiss Seismological Service, ETH Zurich, Switzerland

ABSTRACT: Site effects are rarely considered for earthquake triggering of rock slope failures, however measurements suggest that fracturing of the rock mass within active slope instabilities can amplify shaking by factors of up to 8. At the Randa instability in Switzerland, we measured significant spectral amplification within the unstable rock mass, which we relate through numerical modeling to compliant tension fractures. Slope deformation results in preferential fracture opening, creating meso-scale anisotropy in rock mass moduli. However, another source of damage – preceding earthquakes – also results in systematic fracturing, which can in turn generate site effects in subsequent earthquakes. This feedback is demonstrated in a case study of the Rawilhorn rock avalanche, triggered by the second earthquake of a sequence. We show how the first earthquake damaged the rock mass, opening a number of discontinues, and that this new fracturing created amplified shaking in the next earthquake, likely contributing to failure.

1 INTRODUCTION

Earthquake-triggered landslides are among the most destructive secondary hazards associated with strong seismicity, often resulting in damage to infrastructure and loss of life (Keefer 1984). In addition to properties of the earthquake source and wave path, localized variations in near-surface geotechnical parameters can result in significant amplification or attenuation of ground shaking at different frequencies. These frequency-dependent changes in ground motion are collectively referred to as site effects, and are well known to control distributions of shaking intensity and structural damage in sedimentary basins (e.g. Borchedt & Gibbs 1976, Hough et al. 1990). An increasing number of studies have also shown that site effects can cause significant ground motion amplification even at hard rock sites, in addition to unstable hillslopes, which is related to variable zones of rock weathering or fracturing creating contrasts in seismic wave velocity (e.g. Steidl et al. 1996, Havenith et al. 2002, Bozzano et al. 2011). The growing need to better predict damaging earthquake-triggered slope failures makes recognition and prediction of seismic amplification by site effects on steep hillslopes increasingly critical.

However, to date very few existing studies successfully couple damage created by previous earthquakes – i.e. slope fracturing and weakening of the rock mass – to resulting seismic site effects. Here we attempt to draw a mechanistic link between seismicity, induced rock mass damage, and subsequent site effects, demonstrated through two case studies in the Swiss Alps. We first describe observations at the Randa rock slope instability, where measured spectral amplifications could be linked to the presence of steeply-dipping compliant fractures, demonstrating that slope fracturing generates significant site effects. Then we explore the combined feedback process through a case study of the Rawilhorn rock avalanche, which was triggered by the second strong earthquake of a sequence in 1946. We show through numerical simulation how the first M ~6 earthquake damaged the slope, causing fracture opening within the incipient failure, which was then triggered by the second M ~6 earthquake. Model results demonstrate increased shaking within the instability area, with spectral amplifications increasing by up to a factor of three from the first to the second earthquake.

2 STUDY SITES – RANDA & RAWILHORN

The study region in Canton Valais, Switzerland has a long history of earthquake-triggered slope failures. Nearly every known historical M 6 or greater earthquake has generated at least one damaging rock slide (Fritsche & Fäh 2009), some of which destroyed villages and resulted in loss of life. Widespread rockfalls are also common during each earthquake occurring in this steep alpine landscape.

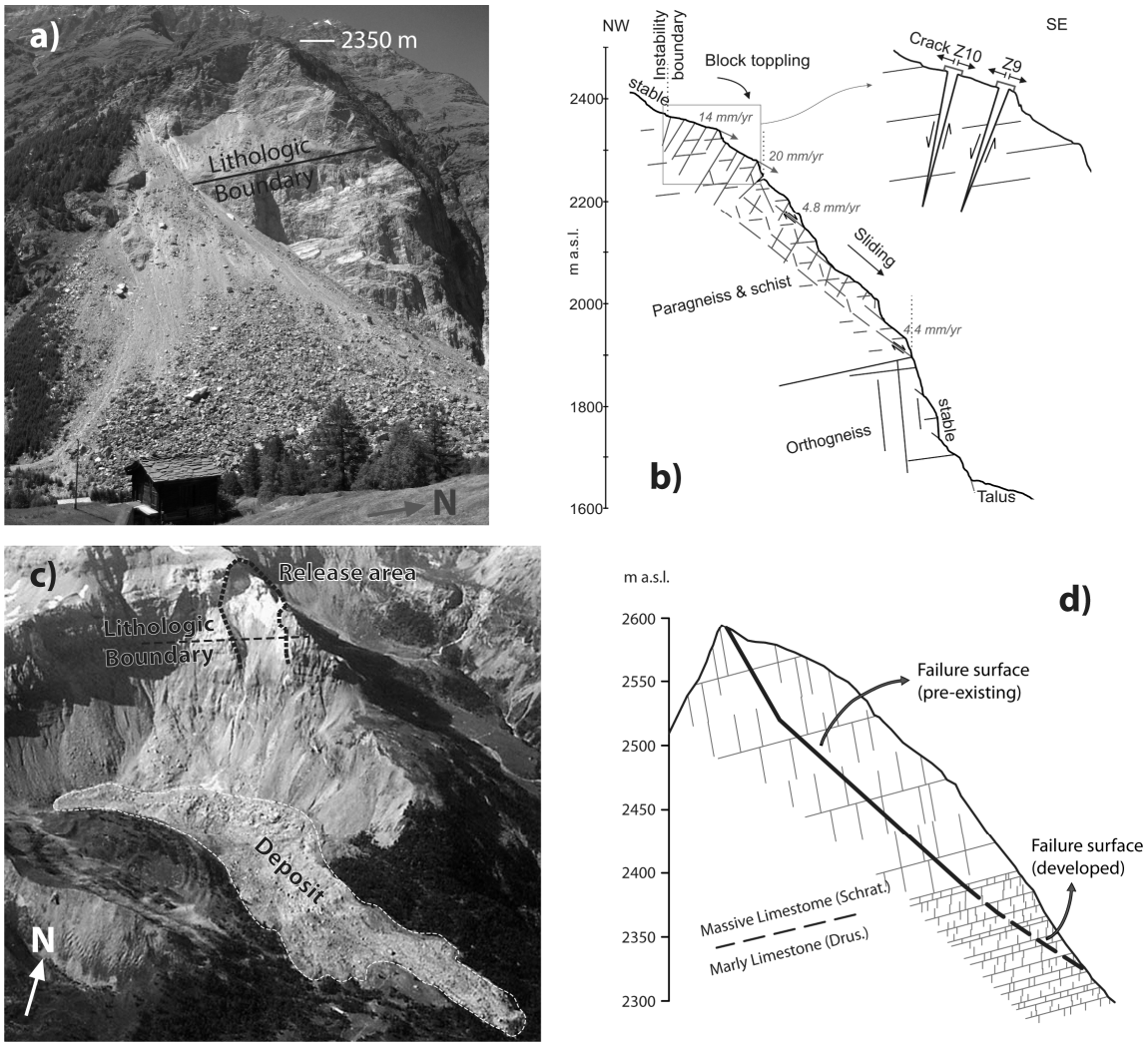

Figure 1: a) Photograph of the Randa slope instability lying behind the scarp of two 1991 failures; the upper part of the slope (above the contact) is currently unstable. b) Geological model of the Randa instability, including the orientation of key discontinuities, kinematic failure modes, and displacement magnitudes. c) Photograph of the 1946 Rawilhorn rock avalanche (source: R. Mayoraz), showing the release area near the ridge, boundary between massive limestone and heavily-fractured marly limestone, and deposit area. d) Geological model of the Rawilhorn failure; two pre-existing faults in the upper limestone form the main portion of the failure surface, which was completed by progressive failure of the supporting toe during the earthquake sequence.

2.1 *Randa rock slope instability*

The current Randa rock slope instability is the legacy of two large failures that occurred in April and May of 1991. Around 5 million m^3 of paragneiss remains unstable today (the upper half of the 1991 failure scarp), moving at rates up to 20 mm/yr (Fig. 1a,b). Underlying this unstable rock mass, a steep orthogneiss cliff shows no evidence of ongoing deformation. Ten years of scientific research at Randa has yielded detailed information on the internal structure and kinematics of the unstable rock mass. The cumulative results of these studies are summarized by Gischig et al. (2011). Borehole logging and surface measurements revealed active fracture zones and their relative displacement rates. A series of steeply-dipping fractures could be traced from the surface to almost 80 m depth to where they intersected a borehole (Willenberg et al. 2008). Large-scale discontinuities delineate blocks, which combine to form compartments in the upper part of the instability. These compartments (or block assemblages) were found to move at similar rates and orientations. Toppling was identified as the dominant failure mode in the upper part of the instability, while translational sliding on a stepped surface is the principle failure mode in the lower area.

2.2 *Rawilhorn rock avalanche*

The last major earthquake in Switzerland (1946 Sierre, M_w 6.1) triggered a number of landslides within the epicentral region (Fritsche & Fäh 2009). Four months later, however, a M_w 6.0 aftershock produced a large rock avalanche from the steep slopes of the Rawilhorn (Fig. 1c,d). The rock avalanche released ~5 million m^3 of sedimentary rock from a ridge approximately 600 m high, and had a run out distance of roughly 1.5 km downstream and 0.7 km upstream. In total there were three strong ($M_w > 5.0$) earthquakes in the vicinity during the months preceding the failure, suggesting an important role of repeated seismic loading in rock mass strength degradation. Post-event analysis showed that the failure

surface consisted of a combination of pre-existing faults and fracture development through an underlying toe (CREALP 2001, Hunziker 2011). In the upper portion of the failure, persistent, pre-existing fault planes bounded large blocks in the massive "*Schrattenkalk*" limestone. The supporting toe material was a heavily fractured and thinly bedded, but competent, marly "*Drusberg*" limestone, with no single thoroughgoing failure plane. Progressive development of a failure surface in the supporting toe likely occurred during the two strong (M ~6) earthquakes, eventually destabilizing the rock mass.

3 RANDA – ROCK FRACTURES AND SEISMIC AMPLIFICATION

3.1 *Measurements*

Between 2002 and 2004, a microseismic monitoring network was installed at Randa (see Spillmann et al. 2007). In addition to capturing microseismic events originating from within the unstable rock mass, the network also recorded signals of nearly 80 regional earthquakes. Instruments employed were 8-Hz, 3-component geophones, distributed around the site in shallow boreholes (Fig. 2). Detected earthquakes had local magnitudes between 0.5 and 2.

In summer 2009, two additional seismometers were deployed at Randa, one within and the other outside of the unstable rock mass (Fig. 2). These 5-s period instruments recorded continuous data intermittently over three months. Seven small regional earthquakes were recorded by these seismometers.

Site effects are commonly quantified using site-to-reference spectral ratios (SRSR), which compare recorded ground motions in different areas against a common reference and as a function of frequency. For microseismic data, station A1 served as the reference, safely outside the unstable area, while seismometer RAND2 was the reference for RAND1. Mean SRSR showing spectral amplification through-out the unstable area are displayed in Figure 2a. These are shown resolved at a frequency of 3 Hz and an orientation of 135°, which was the dominant spectral peak and polarization direction determined from previous analysis of ambient vibrations (Burjanek et al. 2010). Figure 2b shows SRSR for all measurement stations as a function of frequency.

Combined results reveal significant spectral amplification within the unstable rock mass at Randa, with mean spectral ratios reaching factors of up to 8. Amplification is greatest in the area of maximum instability thickness, while outside the unstable area spectral ratios vary marginally around unity. Results thus demonstrate significantly amplified ground motion within the unstable portion of the rock slope in response to small regional earthquakes (weak motions). No large-strain recordings are currently available to study potential non-linear effects.

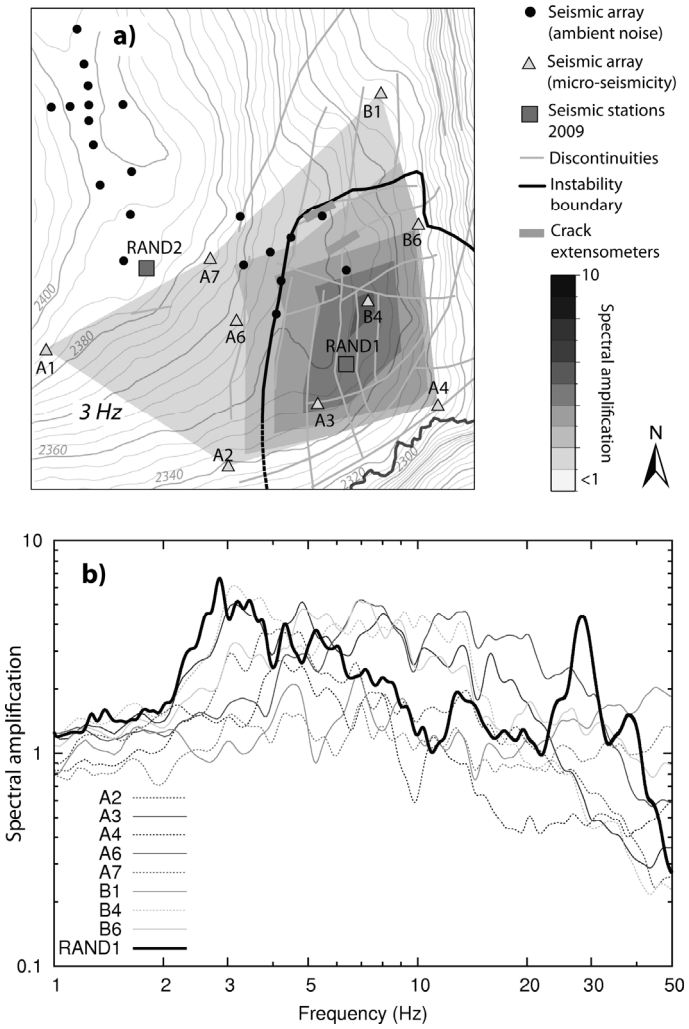

Figure 2: a) Layout of measurements at Randa shown together with key discontinuities and the instability boundary. SRSR calculated from earthquake recordings are shown resolved at 3 Hz and an azimuth of 135°. b) Mean SRSR for all stations as a function of frequency. Modified from Moore et al. (2011).

3.2 *Modeling*

A simplified 2D model of the Randa instability was constructed using UDEC™ (Itasca, Inc.) to study key features of the slope's dynamic response. The model included only mapped steeply-dipping fractures known to include an opening component of dislocation, and these were assigned low shear and normal stiffness values (Fig. 3a). We focus only on elastic behavior, comparing the effect of varying fracture stiffness on the predicted dynamic response.

Figure 3b shows results of our numerical simulation, displaying mean SRSR calculated by comparing the response at five points located both within and outside of the unstable rock mass (see Fig. 3a). Modeled spectral amplifications reach factors of up to 8 at around 3 Hz, which is similar to our measured values. Implementing uniformly stiff fractures, resolved SRSR drop to around unity, signifying no amplification. Thus the observed seismic amplification within the unstable rock mass at Randa could be reproduced simply by including a series of steeply-dipping compliant tension fractures.

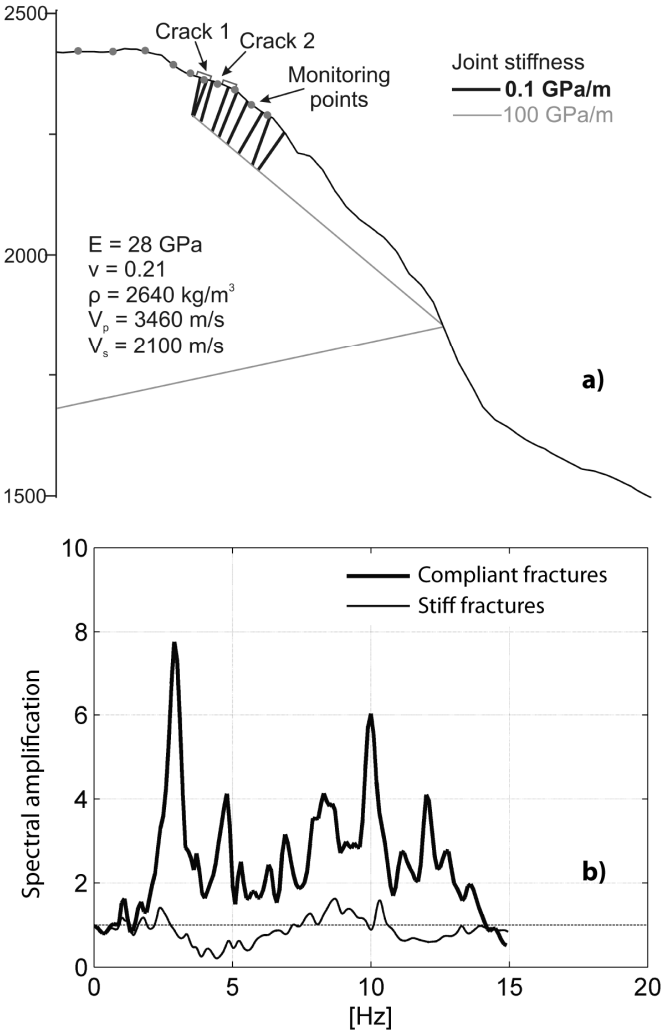

Figure 3: a) Simplified model of the Randa instability implemented in UDEC. b) Modeled spectral amplification comparing stations within and outside the instability and assuming compliant or stiff fractures. Modified from Moore et al. (2011).

Systematic opening of fractures striking subperpendicular to the direction of slope displacement creates meso-scale anisotropy in the bulk rock mass elastic properties – the slope becomes more deformable parallel to the main displacement direction. Such opening-mode fractures are common within active slope instabilities, and our results demonstrate their role in locally amplifying ground motion during small earthquakes; i.e. spatial variations in slope fracturing generate localized seismic site effects.

4 RAWILHORN – COMBINED MODELING OF SLOPE FRACTURING AND SITE EFFECTS

We adopt a three-step procedure to simulate earthquake-induced damage and resulting site effects:

1. Evaluate the dynamic response of the rock slope when all joints are assigned uniformly stiff values.
2. Apply a realistic earthquake input motion and model the distribution of joints that open in tension.
3. Reduce the shear and normal stiffness of these new open joints and again evaluate the dynamic response of the rock slope.

The geometry and select input parameters of the Rawilhorn model implemented in UDEC are shown in Figure 4. Both the Drusberg and Schrattenkalk materials are included and are assigned appropriate elastic properties based on field evaluation of rock mass strength. Different joint networks are adopted for each of the lithologies, reflecting the character of the two rock masses determined from field measurements (Hunziker 2011). Intact blocks between joints have scaled strength and deformability properties to represent the jointed rock mass. The model mesh size was set to 15 m throughout, meaning that frequencies below ~20 Hz are properly sampled.

To evaluate the rock slope's dynamic response, an appropriate input motion is required that uniformly excites the ground over the frequency range of interest (in our case ~1 to 20 Hz). Earthquake recordings are often unsuitable for this purpose since they may contain sporadic spectral information. Rather, we adopt a Ricker wavelet (or a Mexican hat wavelet), which offers both a short time-series input in the form of an analytical solution and a smoothly-varying spectral response (see Fig. 5a).

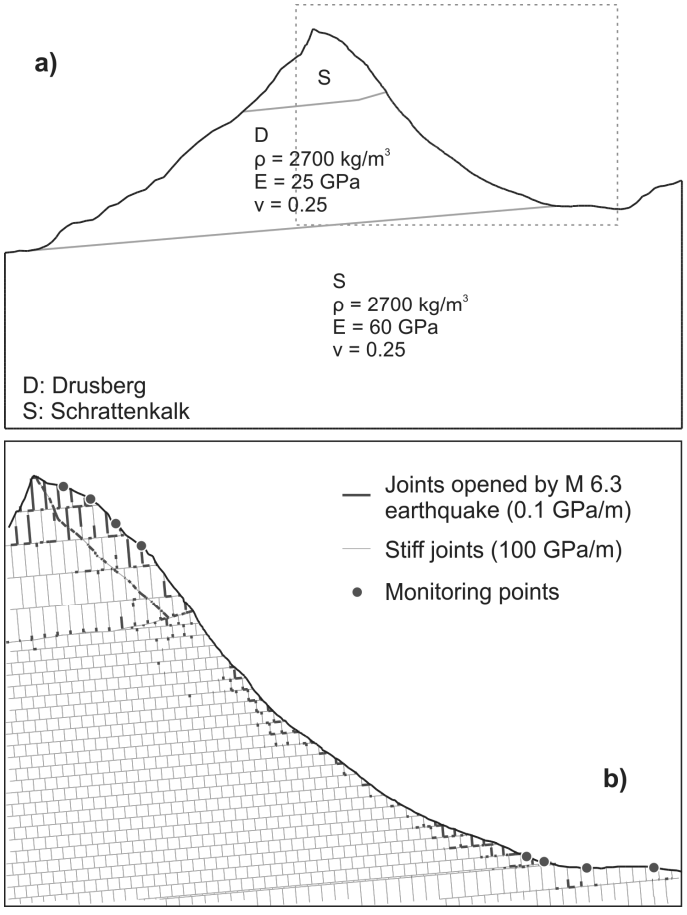

Figure 4: a) Geometry and select properties of the Rawilhorn model implemented in UDEC. b) Detail of the instability area showing open joints after the earthquake simulation, and their corresponding new lower assigned stiffness.

In the first modeling step, all joints are assumed to have high shear and normal stiffness values of 100 GPa/m. Then the Ricker wavelet input motion is applied to the base of the model and the dynamic response evaluated using four ground motion monitoring points both within the incipient instability and on the adjacent valley floor (see Fig. 4b). The average spectral response of the four points near the slope crest is shown in Figure 5a. This spectrum is then set as the baseline against which we can evaluate changes created by including reduced-stiffness joints. This model can also be used to simulate topographic amplification between the slope crest and valley bottom under purely elastic deformation, which we find to be around a factor of 2 on average (c.f. Hough et al. 2010).

In the next step, we simulate earthquake-induced damage and slope fracturing. We concentrate only on modeling joints that open in tension, i.e. those with zero normal stress after the earthquake, as these open fractures are the select few that will have significantly reduced stiffness. This selection also simplifies our simulation strategy. For input motion, we use the recorded ground motion from the 2009 M_w 6.3 L'Aquila earthquake at station AQG, located 4.4 km from the epicenter. This earthquake was a moderate-magnitude shallow-crustal event, and we consider it reasonably similar to that expected in the Valais region of Switzerland and therefore an appropriate input motion for our model. It is also similar in magnitude to those which occurred in 1946 and triggered the Rawilhorn rock avalanche. Both the vertical and one horizontal recording are applied simultaneously to the base of the model.

The distribution of joints that opened in tension after the applied seismic loading (those with zero normal stress after the earthquake) is shown in Figure 4b. These are generally located near the ground surface and preferentially within the upper Schrattenkalk unit near the slope crest. This concentration of open fractures results both from the stiffer nature of the more massive Schrattenkalk rock mass and from topographic effects amplifying ground motion near the crest.

Having predicted the distribution of open joints, we next selectively reduce the stiffness of these fractures (Fig. 4b). In reality, the normal stiffness of an open joint can vary over orders of magnitude, dropping to zero if all wall contact is lost. Most real fractures, however, have rough walls, dispersed asperity contacts and may be filled with collapsed material, giving them non-zero normal stiffness. We chose a value 0.1 GPa/m, consistent with that used for reduced-stiffness fractures in our Randa study.

In the final modeling step, the dynamic response of the slope including reduced-stiffness fractures is evaluated, again using the Ricker wavelet for the basal input motion. These results are shown in Figure 5a, where the spectrum can be compared against the baseline case of uniformly stiff fractures. Figure 5b displays the ratio of these two spectra, quantifying the relative amplification factors resulting from inclusion of reduced-stiffness joints. Notable amplification can be observed, with factors up to 3 at 8 Hz and mean amplification factors of around 1.5 between ~1 and 5 Hz. Relative deamplification also occurs at certain frequencies, especially between 10 and 15 Hz. Larger amplification factors (>3) above 15 Hz may be related to vibration of individual rock mass blocks in our model, which are bounded by compliant fractures.

These results demonstrate how earthquake-induced slope fracturing, which acts to selectively open joints and reduce their normal stiffness, can result in significant spectral amplification during subsequent seismic events. The hypothesized feedback could be reproduced in a series of numerical simulations, lending support to conclusions drawn from our complementary study at Randa. Compliant fractures in damaged or unstable rock slopes can thus be directly linked in both cases to localized relative amplification of ground motion, site effects that may ultimately contribute to earthquake-triggered failure.

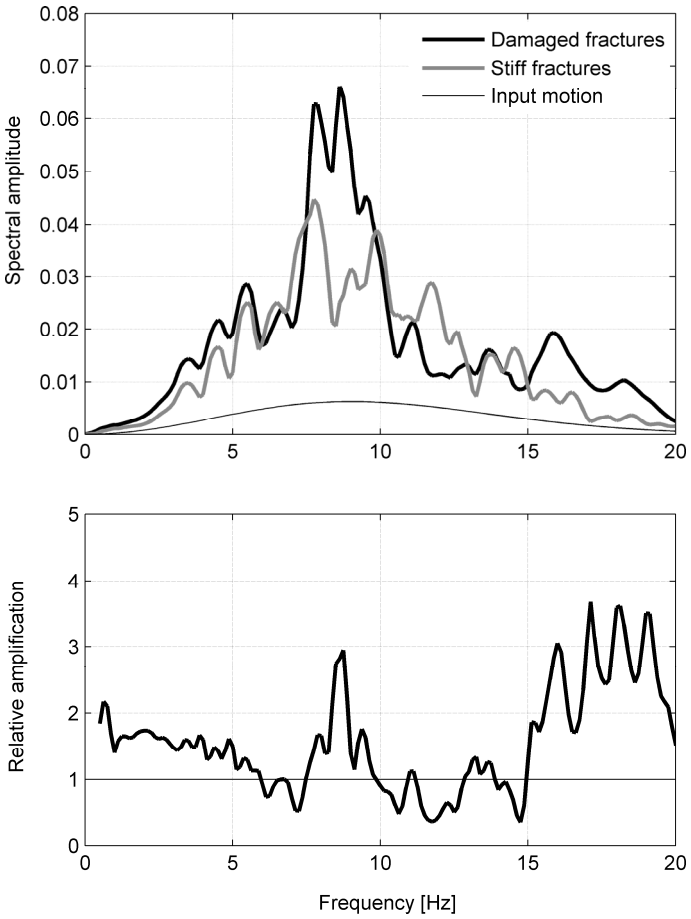

Figure 5: a) Spectra of Ricker wavelet input motion, slope response with uniformly stiff fractures, and response of incipient instability including selectively reduced stiffness fractures resulting from damage (see Fig. 4b). b) Ratio of damaged slope spectra to that from the simulation using uniformly stiff fractures, showing relative spectral amplification.

The Rawilhorn rock avalanche provides a test case to demonstrate our conceptualized feedback between earthquake-induced rock slope damage and seismic site effects. Our simplified modeling procedure was able to reproduce key features of this feedback process. However, we did not attempt to model or quantify actual changes in the slope's factor of safety (FOS) throughout the earthquake succession, which ultimately led to failure. Rather we simply suggest that the FOS will be reduced owing to the simulated damage (new open joints). Then together with the lower FOS, amplified shaking during the next earthquake (caused by site effects) makes the stability situation increasingly unfavorable. As the slope becomes fractured the FOS decreases, meanwhile newly-created compliant discontinuities act to amplify ground motion, and these factors together increase the overall likelihood of subsequent earthquake-triggered failure.

CONCLUSIONS

The combined results of our studies demonstrate the important role of compliant fractures within unstable rock slopes in generating significant spectral amplification during seismic shaking (site effects). These fractures can originate from ongoing slope deformation, as is the case at the Randa instability, or from damage caused by previous earthquakes, as suggested for the Rawilhorn rock avalanche. Fractures with an opening component of dislocation have systematically lower normal stiffness, which results physically from dispersed asperity contacts along fracture walls or collapsed soil infilling. The presence and preferential orientation of opening-mode fractures can often be predicted in case studies by examining local geological information, meaning that site effects, notably spectral amplification (and polarization of ground motion not discussed here), may also be predictable within rock slope instabilities. Our measurements and modeling showed that ground motions may be amplified by factors of up to eight at certain frequencies, meaning that seismic slope stability models ignoring this potentially important effect may underestimate the potential for earthquake-triggered failure.

REFERENCES

Borcherdt, R. & Gibbs, J.F. 1976. Effects of local geological conditions in the San Francisco Bay region on ground motions and the intensities of the 1906 earthquake, *Bulletin of the Seismological Society of America,* 66: 467-500.

Bozzano, F., Lenti, L., Martino, S., Montagna, A., Paciello, A. 2011. Earthquake triggering of landslides in highly jointed rock masses: reconstruction of the 1783 Scilla rock avalanche (Italy), *Geomorphology* 129: 294-308.

Burjanek, J., Stamm, G., Poggi, V., Moore, J.R., Fäh, D. 2010. Ambient vibration analysis of an unstable mountain slope, *Geophysical Journal International*. 180: 820-828.

CREALP. 2001. Eboulement du 30 Mai 1946 du Six des Eaux Froides pres du Rawyl (Valais). Centre de Recherche sur L'Environnement Alpin, Sion, Switzerland.

Fritsche, S. & Fäh D. 2009. The 1946 magnitude 6.1 earthquake in the Valais: site-effects as a contributor to the damage, *Swiss Journal of Geosciences*, 102: 423-439.

Gischig, V., Amann, F., Moore, J.R., Loew, S., Eisenbeiss, H., Stempfhuber, W. 2011. Composite rock slope kinematics at the current Randa instability, Switzerland, based on remote sensing and numerical modeling, *Engineering Geology,* 118: 37-53.

Havenith, H.-B., Jongmans, D., Faccioli, E., Abdrakhmatov, K., Bard, P.-Y. 2002. Site effect analysis around the seismically induced Ananevo rockslide, Kyrgyzstan, *Bulletin of the Seismological Society of America,* 92: 3190-3209.

Hough, S.E., Friberg, P.A., Busby, R., Field, E.F., Jacob, K.H., Borcherdt, R.D. 1990. Sediment-induced amplification and the collapse of the Nimitz Freeway, *Nature*, 344: 853-855.

Hough, S.E., Altidor, J.R., Anglade, D., Given, D., Janvier, M.G., Maharrey, J.Z., Meremonte, M., Mildor, B.S-L., Prepetit, C., Yong, A. 2010. Localized damage caused by topographic amplification during the 2010 *M* 7.0 Haiti earthquake, *Nature Geoscience,* 3: 778-782.

Hunziker, M. 2011. The 1946 Rawilhorn rock avalanche: Modeling damage and failure through successive earthquakes, M.Sc. Thesis, Swiss Federal Institute of Technology (ETH), Zurich, Switzerland.

Keefer, D.K. 1984. Landslides caused by earthquakes, *Geological Society of America Bulletin*, 95: 406-421.

Moore, J.R., Gischig, V., Burjanek, J., Loew, S., Fäh, D. 2011. Site Effects in Unstable Rock Slopes: Dynamic Behavior of the Randa Instability (Switzerland), *Bulletin of the Seismological Society of America*, 101: 3110-3116.

Spillmann, T., Maurer, H., Green, A.G., Heincke, B., Willenberg, H., Husen, S. 2007. Microseismic investigation of an unstable mountain slope in the Swiss Alps, *J. Geophys. Res.,* 112: B07301, doi:10.1029/2006JB004723.

Steidel, J.H., Tumarkin, A.G., Archuleta, R.J. 1996. What is a reference site? *Bulletin of the Seismological Society of America,* 86: 1733-1748.

Willenberg, H., Loew, S., Eberhardt, E., Evans, K., Spillmann, T., Heincke, B., Maurer, H.-R., Green, A. 2008. Internal structure and deformation of an unstable crystalline rock mass above Randa (Switzerland): Part I – Internal structure from integrated geological and geophysical investigations, *Engineering Geology,* 101: 1-14.